LUND UNIVERSITY

Bulk and surface characterization of In2O3(001) single crystals

Hagleitner, Daniel R.; Menhart, Manfred; Jacobson, Peter; Blomberg, Sara; Schulte, Karina; Lundgren, Edvin; Kubicek, Markus; Fleig, Juergen; Kubel, Frank; Puls, Christoph; Limbeck, Andreas; Hutter, Herbert; Boatner, Lynn A.; Schmid, Michael; Diebold, Ulrike

Published in:
Physical Review B (Condensed Matter and Materials Physics)

DOI:
10.1103/PhysRevB.85.115441

2012

Link to publication

Citation for published version (APA):
Hagleitner, D. R., Menhart, M., Jacobson, P., Blomberg, S., Schulte, K., Lundgren, E., Kubicek, M., Fleig, J., Kubel, F., Puls, C., Limbeck, A., Hutter, H., Boatner, L. A., Schmid, M., & Diebold, U. (2012). Bulk and surface characterization of In2O3(001) single crystals. *Physical Review B (Condensed Matter and Materials Physics)*, *85*(11), Article 115441. https://doi.org/10.1103/PhysRevB.85.115441

Total number of authors:
15

General rights
Unless other specific re-use rights are stated the following general rights apply:
Copyright and moral rights for the publications made accessible in the public portal are retained by the authors and/or other copyright owners and it is a condition of accessing publications that users recognise and abide by the legal requirements associated with these rights.
• Users may download and print one copy of any publication from the public portal for the purpose of private study or research.
• You may not further distribute the material or use it for any profit-making activity or commercial gain
• You may freely distribute the URL identifying the publication in the public portal

Read more about Creative commons licenses: https://creativecommons.org/licenses/

Take down policy
If you believe that this document breaches copyright please contact us providing details, and we will remove access to the work immediately and investigate your claim.

LUND UNIVERSITY

PO Box 117
221 00 Lund
+46 46-222 00 00

Download date: 18. May. 2025

Bulk and surface characterization of In_2O_3(001) single crystals

Daniel R. Hagleitner,[1] Manfred Menhart,[1] Peter Jacobson,[1] Sara Blomberg,[2] Karina Schulte,[3] Edvin Lundgren,[2] Markus Kubicek,[4] Jürgen Fleig,[4] Frank Kubel,[4] Christoph Puls,[4] Andreas Limbeck,[4] Herbert Hutter,[4] Lynn A. Boatner,[5] Michael Schmid,[1] and Ulrike Diebold[1,*]

[1]*Institute of Applied Physics, Technische Universität Wien, Wiedner Hauptstrasse 8-10/134, 1040 Wien, Austria*
[2]*Division of Synchrotron Radiation Research, Lund University, Box 118, SE-22100, Sweden*
[3]*MAX IV laboratory, Lund University, Box 118, SE-22100, Sweden*
[4]*Institute of Chemical Technologies and Analytics, Technische Universität Wien, Getreidemarkt 9/164, 1060 Wien, Austria*
[5]*Materials Science and Technology Division, Oak Ridge National Laboratory, Oak Ridge, Tennessee 37831, USA*

(Received 10 November 2011; revised manuscript received 2 February 2012; published 28 March 2012)

A comprehensive bulk and surface investigation of high-quality In_2O_3(001) single crystals is reported. The transparent-yellow, cube-shaped single crystals were grown using the flux method. Inductively coupled plasma mass spectrometry (ICP-MS) reveals small residues of Pb, Mg, and Pt in the crystals. Four-point-probe measurements show a resistivity of $2.0 \pm 0.5 \times 10^5$ Ω cm, which translates into a carrier concentration of $\approx 10^{12}$ cm^{-3}. The results from x-ray diffraction (XRD) measurements revise the lattice constant to 10.1150(5) Å from the previously accepted value of 10.117 Å. Scanning tunneling microscopy (STM) images of a reduced (sputtered/annealed) and oxidized (exposure to atomic oxygen at 300 °C) surface show a step height of 5 Å, which indicates a preference for one type of surface termination. The surfaces stay flat without any evidence for macroscopic faceting under any of these preparation conditions. A combination of low-energy ion scattering (LEIS) and atomically resolved STM indicates an indium-terminated surface with small islands of 2.5 Å height under reducing conditions, with a surface structure corresponding to a strongly distorted indium lattice. Scanning tunneling spectroscopy (STS) reveals a pronounced surface state at the Fermi level (E_F). Photoelectron spectroscopy (PES) shows additional, deep-lying band gap states, which can be removed by exposure of the surface to atomic oxygen. Oxidation also results in a shoulder at the O *1s* core level at a higher binding energy, possibly indicative of a surface peroxide species. A downward band bending of 0.4 eV is observed for the reduced surface, while the band bending of the oxidized surface is of the order of 0.1 eV or less.

DOI: 10.1103/PhysRevB.85.115441 PACS number(s): 68.47.Gh, 68.37.Ef, 71.20.Ps, 61.66.Fn

I. INTRODUCTION

Indium oxide, In_2O_3, has drawn increased attention from researchers over recent years. When doped with SnO_2, the material is commonly referred to as indium tin oxide (ITO), which is the prototypical transparent conducting oxide (TCO). ITO combines high optical transparency in the visible range with an electrical conductivity approaching that of a metal.[1] As a consequence of its interesting physical and chemical characteristics, it is widely used in several technical applications, including transparent films for organic light emitting diodes (OLEDS) and organic photovoltaic cells (OPVC), gas sensing, and transparent infrared reflectors. In_2O_3 is also used in heterogeneous catalysis[2] and in chemical gas sensing.[3] Despite its technological importance, surprisingly little is known about the fundamental surface properties of ITO or those of pure In_2O_3. Even basic material characteristics, such as the fundamental band gap, have been settled only recently.[4,5] The use of a value of 3.75 eV[6] for In_2O_3 (which is the optically determined band gap) instead of the actual value of 2.93 ± 0.15 eV[4] has led to many incorrect conclusions, especially regarding band bending effects and defect chemistry.

So far, samples have been produced mainly by magnetron sputtering, evaporation, or by pressing pellets of powder, which usually leads to polycrystalline, highly defective samples,[7] although new information could be gained from epitaxially grown In_2O_3 and ITO thin films.[4,8–10] In the present work, high-quality single crystals of In_2O_3 are examined.

In_2O_3 is an n-type semiconductor. The n-type conduction arises from intrinsic donor defects, which is related to the pronounced nonstoichiometry observed under highly reducing conditions.[11] To date, In_2O_3 has been regarded as a very good conductor even without extrinsic dopants with a high carrier concentration.[12] Very recent work[13] indicates, however, that surface effects might be mainly responsible for the high conductivity of In_2O_3.

In_2O_3 can exist in three different modifications. In this work, only single-crystal samples crystallized in the bixbyite structure (space group $Ia\bar{3}$) are utilized. The bixbyite structure can be derived from a $2 \times 2 \times 2$ fluorite lattice.[14] To obtain the bixbyite structure, 12 oxygen atoms per unit cell are removed from the anion sublattice in a systematic way. Each {001} anion layer contains four of these vacant oxygen positions. The cubic unit cell of In_2O_3 has, according to the literature,[15] a lattice parameter of 10.117 Å (for a revised value see Sec. II A 2) and consists of 80 atoms—32 indium atoms and 48 oxygen atoms (Fig. 1). Two distinct indium positions with different symmetries can be found in the crystal. These are commonly referred to as In-b (8 atoms per unit cell) and In-d (24 atoms). The In-b sites are axially symmetrically coordinated, and the In-d sites present high asymmetry in their coordination. Along the (001) direction, the crystal can be thought of as a stack of three different layers. These can be identified as a mixed layer, which consists of In-b and In-d atoms (M-layer), a layer containing In-d atoms only (D-layer), and an oxygen layer. An important characteristic of In_2O_3(001) is the polarity of its surface (Tasker type-III):[16,17]

 ©2012 American Physical Society

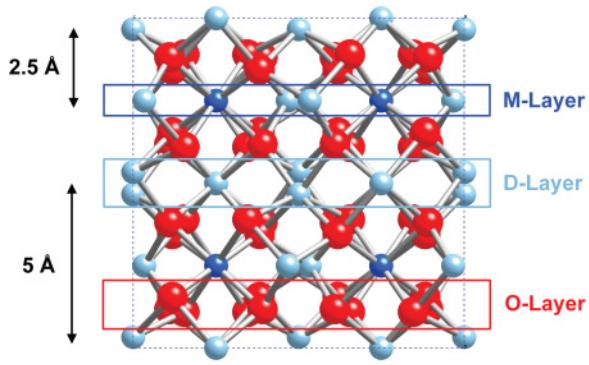

FIG. 1. (Color online) Unit cell of the In_2O_3 bixbyite structure. Large (red/dark gray) balls are oxygen, and small blue balls are In-b (medium gray) and In-d (light gray).

The alternating indium and oxygen layers lead to a net dipole moment perpendicular to the surface. However, polar surfaces cannot have bulk-like surface terminations; in this case, the electrostatic potential would diverge for a macroscopic material. A depolarization field is required to stabilize the surface. This can be achieved by different mechanisms such as reducing the top and bottom layer surface charges, changes in surface stoichiometry, surface reconstructions, adsorption, or faceting.[17] Recent scanning tunneling microscopy (STM) measurements of epitaxial ITO films showed that the nonpolar (111) surface has a 1×1 structure with a simple bulk-like termination,[8] while the polar (001) surface is considerably more complex.[9] These previous measurements were, however, complicated by the fact that (001)-oriented In_2O_3 films tend to facet, which leads to rough surfaces.[10] The availability of high-quality, (001)-oriented single crystals, in combination with a recent density functional theory (DFT) work[18] that describes possible terminations of low-index In_2O_3 surfaces, has motivated us to undertake the present study.

II. EXPERIMENTS

A. Bulk characteristics

1. Crystal growth

The crystals were grown using the flux method. The flux (solvent) used was B_2O_3 and PbO. In addition, a small amount of MgO was added. This mixture of In_2O_3, B_2O_3, PbO, and MgO powders was melted in a platinum crucible and maintained at a temperature of 1200 °C for 4 to 10 hours. The temperature was then programmed to decrease by 3 °C per hour. As soon as a temperature of 500 °C was reached, the furnace was turned off. The crystals were extracted from the solidified flux using a 1:4 solution of HNO_3 and water. The resulting cubic crystals are yellow-transparent and have side lengths between 1 and 2 mm, as shown in Fig. 2. Polarized-light microscopy showed that the crystals can be characterized as heterogeneous single crystals with multiple growth domains and stress birefringence (see Fig. 2).

2. Determination of impurity levels

Inductively coupled plasma mass spectrometry (ICP-MS) measurements were performed to determine whether the crystals have residues from the flux or show other contaminations. The measurements were performed using an NWR-213 laser ablation system from New Wave Research (ESI, Fremont, CA) coupled to an X-Series 2 ICP-MS System from Thermo Fisher Scientific (Bremen, Germany). In total, 18 different spots were ablated to minimize the influence of local irregularities in the sample. Trace impurities were quantified using a mass balance model based on the assumption that the target is 100% In_2O_3 with a natural isotope distribution. Element concentrations were calculated from the acquired intensity counts with reference to the ^{113}In signal and the respective natural isotope abundance. Results were averaged from all 18 measurements. The highest concentrations were found for Pb (4307 ± 74 ppm), Mg (1388 ± 42 ppm), and Pt (155 ± 28 ppm). Trace amounts (<50 ppm) of Zr, Sn, Sb, Nd, and Bi were identified. Boron has a low signal intensity in ICP-MS, and only a small amount was detected.

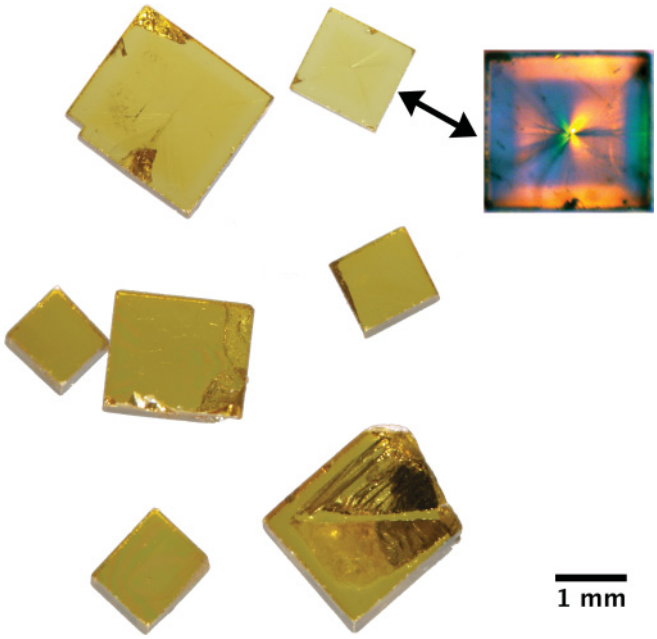

FIG. 2. (Color online) The investigated In_2O_3 single crystals. A polarized light microscope image of one of the crystals is shown at the right.

The time-of-flight secondary ion mass spectrometry (TOF-SIMS) measurements were carried out on a TOFSIMS.5 (ION-TOF GmbH, Münster, Germany) instrument. Depth profiles (∼2000 nm) for the most abundant impurities in the crystals (Pb, Mg, Pt) showed a homogeneous distribution and no significant reduction of intensity with sputter time.

3. X-ray diffraction

A small fragment broken from the corner region of the platelet was used for single-crystal analysis. This crystal was controlled optically and showed no birefringence or domains. Structure analysis was made using a Bruker SMART diffractometer with a graphite monochromator and a SMART APEX detector using molybdenum K_α radiation ($\lambda = 0.71073$ Å) at room temperature (293 K). Frames were integrated using SAINT PLUS (Bruker, 2008) and absorption correction was performed using a multiscan approach with SADABS (Bruker,

TABLE I. In_2O_3 atomic coordinates determined by XRD. The occupation of all sites is 1.

Site	Wyckoff symbol	X	Y	Z
In1	8b	0.25	0.25	0.25
In2	24d	0.466393(2)	0	0.25
O	48e	0.39037(2)	0.15470(2)	0.381852(19)

2008). The lattice parameters and systematic extinctions clearly indicate a cubic space group $Ia\bar{3}$. The unit cell size was determined to 10.1150(5) Å. The structure analysis was made using the XTAL refinement package[19] and converged to R = 0.017. The atomic coordinates are given in Table I. Details of the refinement are given in Table II, atomic displacement parameters can be found in Table III, and interatomic distances are provided in Table IV. The data were deposited at the Cambridge Crystallographic Data Centre (deposition number CCDC 846726).

4. Resistivity measurements

The resistivity of the In_2O_3 crystals was measured in an ambient atmosphere after a temperature excursion to 500 °C. We used the four-point-probe method with AC voltage (frequency range: 1–10 Hz). The resistivity at room temperature is $(2.0 \pm 0.5) \times 10^5$ Ω cm.

B. Surface characteristics

1. Surface quality

The sample surface preparation consisted of several sputtering and annealing cycles in an ultra-high vacuum (UHV) chamber (base pressure $<5 \times 10^{-10}$ mbar). A sputtering cycle included a 10 minute surface bombardment with 2 keV argon ions (current density $\approx 10^{-5}$ A/cm^2). Thereafter, the sample was annealed at 500 °C for 10 minutes in UHV. Annealing to higher temperatures (600 °C) caused an irreversible color change of the crystal to orange and was therefore avoided; such a change is likely caused by the desorption of oxygen and the formation of additional oxygen vacancies.[20] For some experiments, an oxidized surface was prepared by exposing the sample to activated oxygen from an atomic oxygen source (Oxford Applied Research Thermal Gas Cracker TC-50; oxygen pressure: 2.5×10^{-7} mbar) for 30 minutes at a sample temperature of 300 °C.

TABLE II. Refinement parameters.

Refinement on F^2
$R[F^2 > 2\sigma(F^2)] = 0.016$
$wR(F^2) = 0.017$
$S = 3.61$
910 reflections
18 parameters
Weighting scheme based on measured s.u.'s $1/\sigma^2$
$(\Delta/\sigma)\max = 0.20$
$\Delta\rho_{\max} = 2.66$ e Å^{-3}
$\Delta\rho_{\min} = -2.77$ e Å^{-3}

After several initial sputtering and annealing cycles, the surface showed a sharp low-energy electron diffraction (LEED) pattern as shown in Fig. 3(a). These results compare well with the LEED results reported earlier by Morales and Diebold,[9] which were obtained on pure and tin-doped In_2O_3 (001) thin films grown with oxygen-plasma–assisted molecular beam epitaxy (MBE) on yttria-stabilized zirconia (YSZ). Similar to their results, a p4g glide plane symmetry is observed, which causes the extinction of the (0, n + 1/2) and (n + 1/2, 0) spots indicated by white boxes in Fig. 3(a). LEED images of the oxidized surface showed the same pattern. In particular, no signs of faceting (streaking and spot splitting while changing the beam energy) could be observed.

Auger electron spectroscopy (AES), x-ray photoelectron spectroscopy (XPS), and low-energy ion scattering (LEIS) with 1 keV helium ions and a scattering angle of 137° confirmed that the surface was free of contamination. LEIS, which is sensitive to strictly the top-most layer, showed an indium peak that was far larger than the oxygen peak [Fig. 3(b)]. Oxidization of the surface drastically reduced the indium signal, which means the indium layer was probably covered by oxygen. The small height of the oxygen peak is attributed to the high neutralization of the He^+ ions by negatively charged oxygen at the surface.

2. STM

Scanning tunneling microscopy (STM) was performed in UHV (base pressure $<5 \times 10^{-10}$ mbar) at room temperature with three different instruments (SPECS Aarhus design, a customized Omicron micro-STM, and an Omicron STM-1) using electrochemically etched tungsten tips. Imaging was possible with both positive and negative bias, and there is no apparent difference in the appearance of atomically resolved images.

A 100×100 nm^2 image of the sputtered/annealed (reduced) surface is shown in Fig. 4. It exhibits wide terraces with step edges preferably aligned in the [110] directions. The line profile shows that the terraces have a step height of 5 Å.

Figure 5(a) shows a 20×15.75 nm^2 image with higher resolution. It is dominated by bright, atomic-sized protrusions, which at first seem to be arranged in a disordered way. Analysis of the Fourier transform, however, clearly reveals a square 3.6 Å lattice; this length equals a quarter of the diagonal of the In_2O_3 bulk unit cell. We have extracted this lattice by first creating a binary image with only one nonzero pixel at the center of each atom. We have then filtered this binary image in the Fourier domain, keeping only the spatial frequency components corresponding to the 3.6 Å periodicity. The resulting lattice positions are shown as dots in Fig. 5(b). It is obvious that most atoms are close to a lattice site on this regular 3.6 Å grid but are not directly on it. Only a few atoms are far from lattice sites, sometimes close to the center of a grid cell. The coverage of the protrusions in Fig. 5 amounts to about two per unit cell, which is one-quarter of the atomic density of the 3.6 Å lattice. The dark areas without protrusions are situated 2.5 Å below the protrusion level.

After exposing the sputtered/annealed surface to atomic oxygen, the same step height distribution was found. The terraces visible in Fig. 6(a) have a height difference of

TABLE III. Atomic displacement components.

Site	Wyckoff symbol	U^{11}	U^{22}	U^{33}	U^{12}	U^{13}	U^{23}
In1	8b	0.004290(9)	0.004290(9)	0.004290(9)	0.000580(5)	0.000580(5)	0.000580(5)
In2	24d	0.003971(11)	0.004030(10)	0.004162(10)	0	0	0.000542(5)
O	48e	0.00615(5)	0.00592(5)	0.00511(5)	−0.00046(4)	−0.00096(4)	−0.00027(4)

∼5 Å. In higher-resolution images, the surface appears more rough and complex [Fig. 6(a)] than the reduced surface. The overall morphology of the surface is unchanged, however, with relatively large, flat terraces, and, again, no indication of surface faceting. For both preparation conditions, the appearance is the same for empty- and filled-state tunneling conditions.

3. STS

STS was applied to measure the local density of states (LDOS) of the sample around E_F. In total, 400 spectroscopy points from a 20 × 20 grid in a 30 × 30 nm^2 area were acquired. A lock-in amplifier was used to directly obtain the differential conductance dI/dV, which is roughly proportional to the LDOS. The STS spectrum in Fig. 7 shows the average over the 400 dI/dV curves. A strong state at E_F is clearly visible.

4. PES

High-resolution photoelectron spectroscopy (PES) was carried out at the MAX II storage ring at MAX-lab in Lund, Sweden. The SX-700 monochromator at beamline I311 supplies photons in the energy range from 43 to 1500 eV.[21] The spectroscopy end station is used for high-resolution XPS and NEXAFS measurements under UHV conditions (base pressure: $<3 \times 10^{-10}$ mbar). The preparation chamber includes, among others, an argon ion sputter gun, LEED optics, mass spectrometer, and an atomic oxygen source. A hemispherical energy analyzer (SCIENTA SES200) was used for the photoemission experiments. Measurements were performed at room temperature with the photon beam incident at 55° to the sample surface and normal emission.

For these measurements, the In_2O_3 crystal was directly mounted on top of a rhodium crystal. This allowed us to calibrate the Fermi energy with an accuracy of ±0.01 eV by measuring the sharp Fermi edge of the rhodium surface next to the In_2O_3 sample. E_F is defined as 0 eV binding energy for all of the spectra shown here. Due to the small size of the In_2O_3 crystals, it was difficult to completely avoid rhodium peaks; the rhodium counts could be minimized to about 1% of the In $3d_{5/2}$ counts. For most measurements, a photon energy of 105 eV was chosen because the Rh *4d* levels have a cross-section minimum at this energy.[22]

TABLE IV. Interatomic distances.

In2-O1(2)	2.1952(2)	In1-O1(6)	2.1734(2)
In2-O1(2)	2.2236(2)	In1-In2(6)	3.34447(12)
In2-In2(4)	3.36170(12)	In1-In2(6)	3.82412(14)
In2-O1(2)	3.8167(3)	In1-O1(6)	3.9926(3)
In2-In2(4)	3.83920(14)	In2-O1(2)	2.1249(2)

Sample preparation was identical to that used for STM analysis. To oxidize the surface, an OBS-40 gas cracker (MBE Komponenten, Weil, Germany) was used. The crystal was treated with atomic oxygen for 30 minutes at an oxygen pressure of 3×10^{-7} mbar and a flux of $\sim 5 \times 10^{14}$ oxygen atoms cm^{-2} s^{-1}. While dosing, the sample was kept at a temperature of 200 °C or 400 °C.

Figure 8(a) shows a comparison of the valence band (VB) of the reduced and oxidized surfaces. The valence band maximum (VBM) was determined by extrapolating a linear fit of the leading edge of the valence band photoemission to the background level.[23] The VBM was determined using the data displayed in Fig. 8(a) and lies at 2.9 eV and 2.4 eV below E_F for the reduced and the oxidized surfaces, respectively. A shift of the same magnitude can be seen for the In $3d_{5/2}$ core levels [0.52 ± 0.11 eV; Fig. 9(a)] and the O *1s* core level [0.54 ± 0.11 eV; Fig. 9(b)]. The In *4d* semicore levels are shifted by a smaller amount (≈0.3 eV); they are probably influenced by the VB.

A closer look at the O *1s* peak of the oxidized surface reveals a shoulder at higher binding energy, shifted by 1.8 eV with respect to the main peak, as shown in Fig. 9(c). Further noteworthy features in Fig. 8(a) are the pronounced gap states of the sputtered/annealed surface, which completely disappear for the oxidized surface.

Figure 8(b) shows the VB of the reduced surface at different photon energies. The intensity of the gap states decreases with increasing photon energy, i.e., with decreasing surface sensitivity.

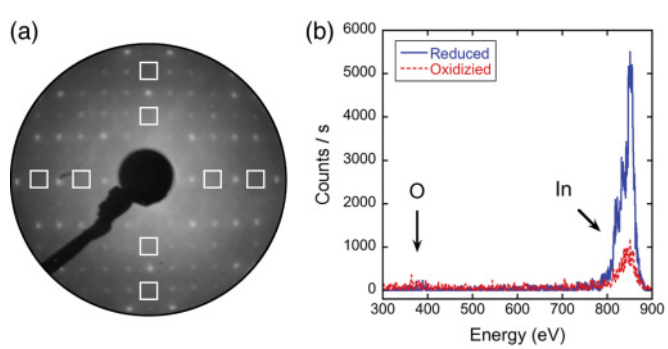

FIG. 3. (Color online) (a) LEED image of an In_2O_3(001) single crystal ($E_{Electron}$ = 100 eV) prepared by sputtering and annealing. Squares mark the (0, n + 1/2) and (n + 1/2, 0) spots that are missing due to the *p4g* glide plane symmetry. (b) LEIS spectra (1 keV He$^+$) of the sputtered/annealed (reduced) and oxidized surface.

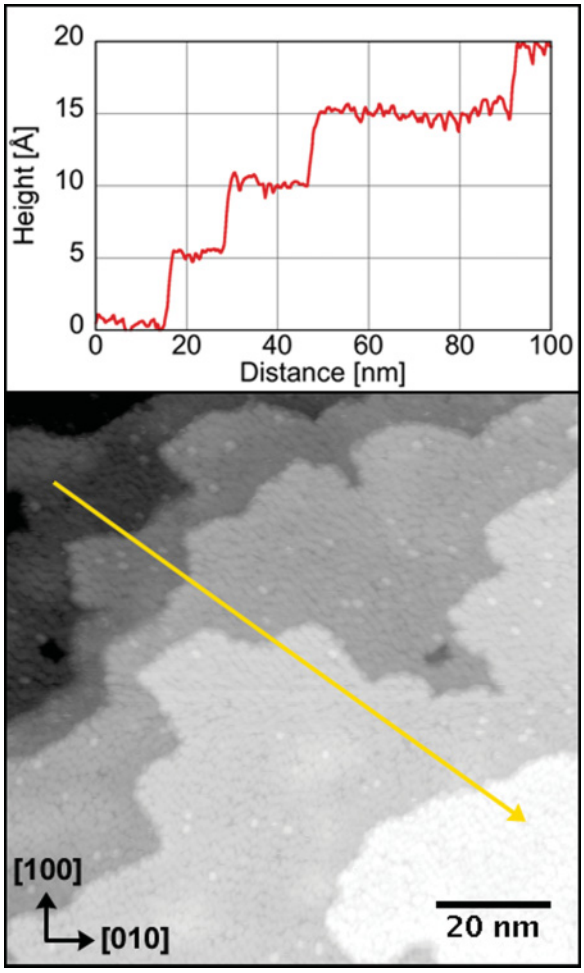

FIG. 4. (Color online) STM image of a sputtered/annealed $In_2O_3(001)$ surface taken with a sample bias of $V_{Sample} = -3$ V and tunneling current $I_{Tunnel} = 0.23$ nA. The arrow indicates the location of the line profile.

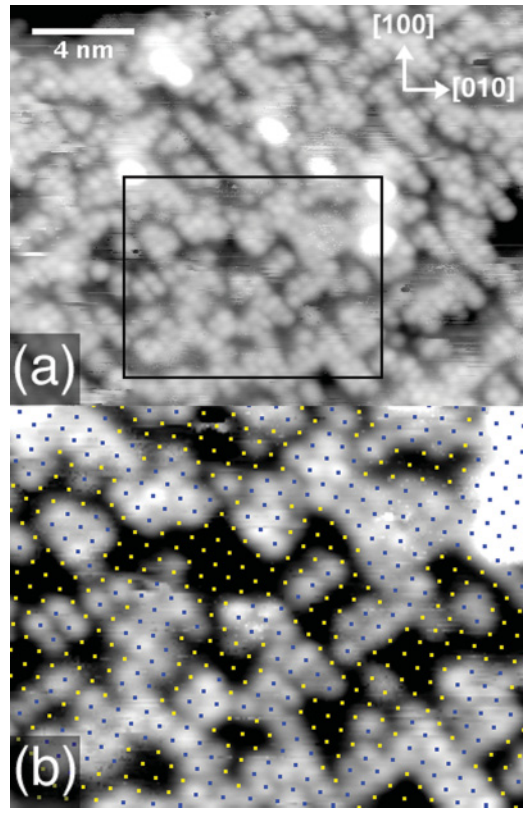

FIG. 5. (Color online) (a) STM image of the reduced surface with atomic resolution ($V_{Sample} = -2.6$ V, $I_{Tunnel} = 0.17$ nA). (b) A magnification of the framed part indicated in (a). The 3.6 Å lattice obtained from the Fourier transform is overlaid.

III. DISCUSSION

A. Surface structure

As shown in Sec. II B 2, all the step edges of both the sputtered/annealed (i.e., reduced) and oxidized $In_2O_3(001)$ surfaces have a height 5 Å. This has an important consequence if one considers the crystal structure of In_2O_3 (Fig. 1): The distance between equivalent layers (e.g., from M- to M-layer) is roughly 5 Å. However, adjacent layers (i.e., from M- to D-layer) have a distance of about 2.5 Å. The observation of 5-Å-high steps implies that the large terraces have one particular termination, either M or D. On the other hand, the atom-sized protrusions on the reduced surface (Fig. 5) appear on a background ~2.5 Å lower, which indicates a coexistence of two terminations on a very small scale. Also, the even larger spread of heights of the oxidized surface indicates a coexistence of different terminations on that surface.

In a recently published paper by Agoston and Albe,[18] possible terminations for low-index In_2O_3 surfaces were investigated in detail by DFT calculations. Both, stoichiometric (i.e., half of the indium or oxygen atoms missing from the bulk-terminated surfaces that are shown in Fig. 10) and nonstoichiometric surfaces were considered as a function of the oxygen chemical potential. For the stoichiometric surfaces, these calculations show that the half-oxygen terminations are energetically preferable compared to the half-indium terminations, in agreement with previous DFT results from Walsh and Catlow.[1] The differences are very small, however. Due to the small energy differences between the different terminations, Agoston and Albe concluded that considerable disorder has to be expected and that even a coexistence of different terminations could be possible.

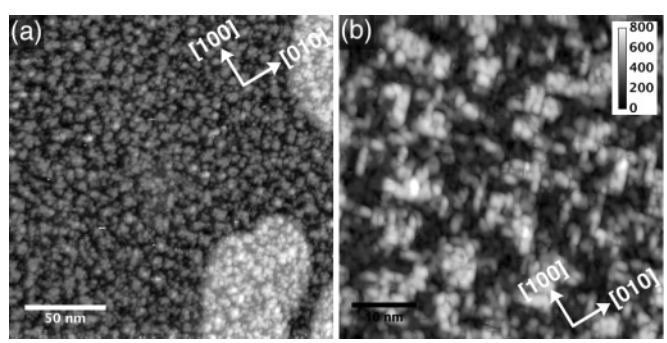

FIG. 6. STM images of the oxidized surface taken at (a) $V_{Sample} = +2.3$ V, $I_{Tunnel} = 0.25$ nA, and (b) $V_{Sample} = +1.8$ V, $I_{Tunnel} = 0.25$ nA. The calibration bar in (b) shows that the surface is rough at the atomic scale (height units: pm).

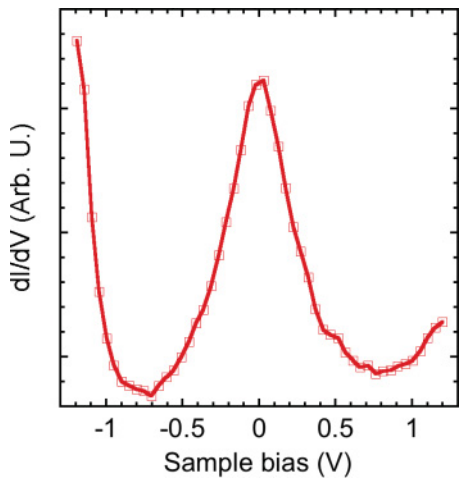

FIG. 7. (Color online) Scanning tunneling spectroscopy of a sputtered/annealed $In_2O_3(001)$ surface.

The surface stoichiometry depends on the oxygen chemical potential. Agoston and Albe found that different surface terminations become energetically preferable when going from highly reducing to highly oxidizing conditions: (i) additional indium nucleates on top of the surface; (ii) 2 oxygen atoms per unit cell (M-layer), (iii) 4 oxygen atoms per unit cell (D-layer); (iv) stoichiometric termination with six surface oxygen atoms; (v) partially dimerized termination with two dimers (i.e., peroxo species) and 4 oxygen atoms; and (vi) 6 dimers (M-layer). A dimerized surface would be in agreement with other DFT calculations, which predict that surface oxygen atoms undergo a dimerization.[3,24]

For the sputtered/annealed surface, we can safely rule out a (partial) peroxide termination for the following reasons: (i) The preparation included annealing to 800 K in an oxygen background pressure of less than 10^{-12} mbar. This corresponds to an oxygen chemical potential of approximately -2 eV, assuming equilibrium with the residual gas. This would lead to a metallic termination according to Ref. 18. (Due to kinetic limitations, the actual surface composition will be slightly closer to the oxygen-rich side, however.) (ii) Oxygen has been depleted by sputtering. (iii) The top layer consists predominantly of indium according to LEIS [Fig. 3(b)]. (iv) According to simulated STM images, oxygen dimers should appear dark.[18] (v) As suggested by Gassenbauer *et al.*,[25] a surface peroxo species should show an O *1s* core level with an additional structure at the higher binding energy (BE) side. While we, indeed, see such a peak for the oxidized surface in Fig. 9(c), it is absent for the sputtered/annealed surface.

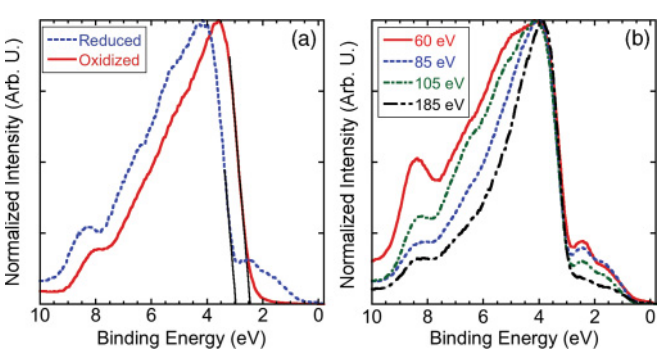

FIG. 8. (Color online) (a) Normalized valence band spectra of the oxidized and sputtered/annealed $In_2O_3(001)$ sample at 105 eV photon energy. Linear extrapolations for determining the leading edge of the valence band (VB) are indicated. (b) VB of the reduced surface at different photon energies.

At first sight, the atom-sized features in Fig. 5(a) seem to be arranged in an unsystematic way. As shown in Fig. 5(b), most protrusions (atoms) of the reduced surface are close to lattice sites of a 3.6 Å lattice, rotated by 45° with respect to the axes of the unit cell. The ball models in Fig. 10 show the bulk-terminated layers of the (i) D-Layer, (ii) M-layer, and (iii) O-layer with all the indium and oxygen atoms present. Figure 9(c) shows that all oxygen atoms are situated close to lattice sites of a square lattice with $a/4 \approx 2.5$ Å, aligned with the axes of the unit cells. We examined whether the protrusions visible in the STM image (Fig. 5) could fit to such an O-layer lattice, but we found no solution that is compatible with the fourfold symmetry of the surface. The arrangement of the indium atoms is a distorted 3.6 Å lattice rotated by 45°, for both D- and M-terminations [see Figs. 10(a) and 10(b)]. This suggests that the protrusions visible in the STM image of the sputtered/annealed surface are indium atoms, but that this indium lattice is only partially occupied. The number of protrusions in the STM image is ≈2 per unit cell. This corresponds to half the indium atoms expected for a stoichiometric In-terminated surface [or one-quarter of the density of the full indium D- or M-layer shown in Figs. 10(a) and 10(b)].

Comparing the atoms in Fig. 5 with the simulated STM images for the reduced surface (Fig. 12 in Ref. 18), the elongated shape of the atoms could be an indication that we are seeing the D-layer. The unresolved dark areas in Fig. 5, ∼2.5 Å below the protrusions, would then be the M-layer. The surface would thus consist of an M-layer at the base, with small, irregular patches of a D-layer on top. The deviations of the atomic positions from a square 3.6 Å lattice, as seen by STM, are larger than those in either the D- or the M-layer, however, and so they might be related to either a density of states that is not centered at the atoms, or they may be due to mutual repulsion of the positively charged indium atoms distorting the lattice.

The occurrence of small islands on a polar metal-terminated oxide surface is reminiscent of the ZnO(0001) case, where it was found that O-terminated step edges provide additional negative charge, compensating for the excess positive charge of the zinc.[26] We consider it possible that the same mechanism explains the occurrence of the small indium islands on the $In_2O_3(001)$ surface.

According to Ref. 18, the (001) orientation is the most stable one for strongly reducing conditions only. Upon oxidation, one could expect faceting as a stabilization mechanism. Faceting of $In_2O_3(001)$ thin films has been previously reported by others.[9,10,27,28] However, the STM images of the oxidized surface [Figs. 6(a) and 6(b)] together with the LEED measurements clearly show that no macroscopic faceting occurs on our crystals. The height variations seen in the STM images may be considered a kind of faceting on the atomic scale, however, with ubiquitous single or multiple steps, each of

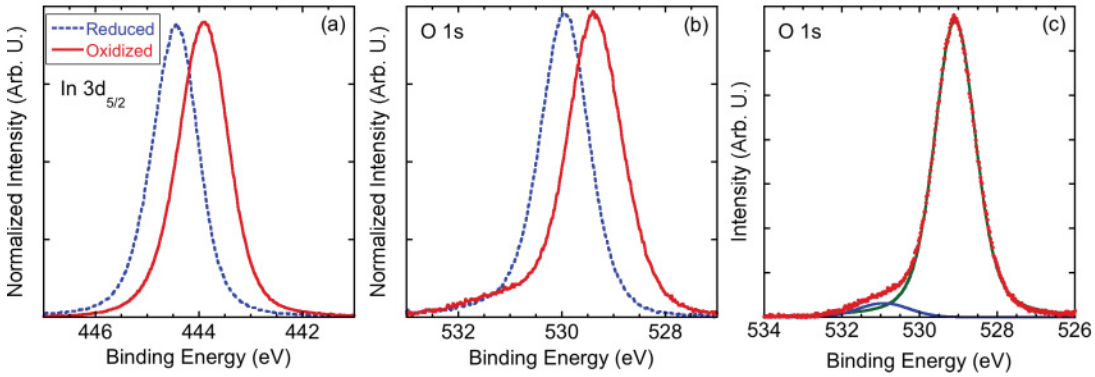

FIG. 9. (Color online) PES on the sputtered/annealed (reduced) and oxidized samples of the (a) In $3d_{5/2}$ and (b) O *1s* core levels, taken with a photon energy of 610 eV. (c) Line fits of the O *1s* peak of the oxidized surface at 610 eV.

them a nanofacet. Unfortunately, this rather rough surface did not allow us to obtain STM images of sufficient resolution to discern details about the step structure. As for the reduced surface, the coexistence of several height levels and small-scale structure with steps has not been anticipated in the DFT studies, and therefore the DFT-derived surface energies cannot accurately describe the real surface.

Further insight about the oxidized surface can be obtained from the photoelectron spectrum of the O *1s* core level: Figure 9(c) shows a shoulder attributed to the presence of peroxide species (cf. Ref. 25). Agoston and Albe[18] considered a "full" peroxide termination (6 dimers/unit cell) and a "partial" peroxide surface (2 dimers, 4 oxygen atoms). Assuming we probed three monolayers with PES (due to the photoelectron escape length at a kinetic energy of ~100 eV), the expected ratio of oxygen in peroxide versus oxygen in bulk-like positions should be ~1/3 and ~1/10 for the full and partial peroxide termination, respectively. The intensity ratio of the shoulder to the main O *1s* peak in Fig. 9(c) amounts to 5.3%. This indicates that the oxidized crystal has a considerably lower peroxide coverage than the full peroxide termination, even lower than the partial peroxide termination considered in Ref. 18.

Interestingly, the STM results presented here show quite a different appearance from the results obtained earlier by Morales and Diebold.[9] They investigated thin films of ITO(001) grown on YSZ and prepared with an oxygen plasma source, i.e., under highly oxidizing conditions. Protrusions arranged in a zigzag pattern were observed and interpreted as oxygen dimers of the peroxide termination. Cross-shaped dark features were attributed to missing dimers. The samples investigated in Ref. 9 differ in various ways from the single crystals studied here: They were grown in a highly oxidizing environment; they consisted of relatively thin epitaxial films that may have been influenced by strain induced by the YSZ substrate; and they were doped with Sn. All three parameters are expected to affect the surface termination, although it is left to future investigations to determine to what extent.

B. Electronic structure

1. Bulk properties

We will initially discuss the results from the four-point-probe measurements. The accuracy of the resistivity values is limited by the fact that no distinction between bulk and surface conductivity is possible. Also, surface states may play a role in the surface conductivity. This makes it difficult to determine the resistivity accurately, but they do give an order of magnitude that will be sufficient for the following considerations.

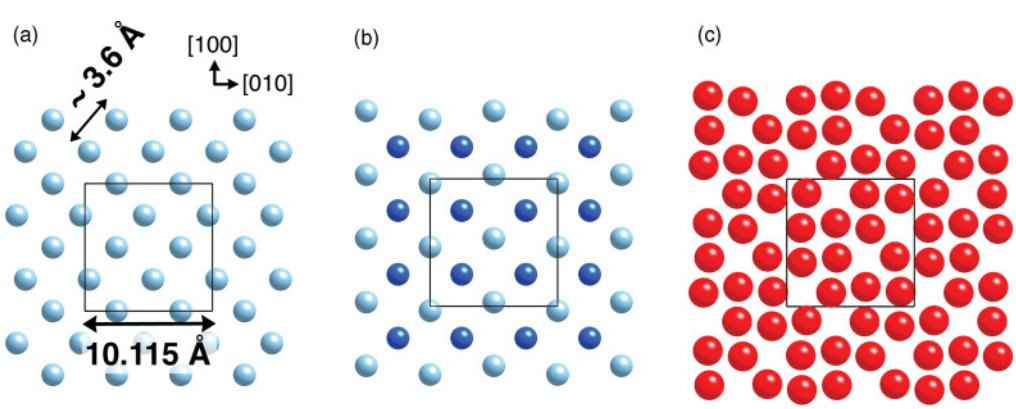

FIG. 10. (Color online) Models of the $In_2O_3(001)$ surfaces with (a) D-layer, (b) M-layer (b), and (c) O-layer termination. Shown are bulk-terminated layers with all the indium and oxygen atoms present; In-b atoms are shown darker than In-b. Note that these terminations represent polar surfaces; for stoichiometric surfaces, only half of the atoms shown here are expected to be present.

The carrier concentration n can be calculated from the conductivity σ and the carrier mobility μ using the relation:[29]

$$n = \frac{\sigma}{e\mu}.$$

The carrier mobility value $\mu = 32\ \mathrm{cm}^2\ \mathrm{V}^{-1}\ \mathrm{s}^{-1}$ was obtained from Ref. 4, and the conductivity σ was taken from our four-point measurements (Sec. II A 4). The carrier concentration then results in $(1.0 \pm 0.2) \times 10^{12}\ \mathrm{cm}^{-3}$, which is almost 5 orders of magnitude smaller than the lowest value reported previously in the literature (see Ref. 30). This means our crystals have fewer impurities than the ones investigated in previous publications. This is emphasized by the fact that our crystals are yellow, compared to the often reported green or black coloration of In_2O_3.[31] An additional reason for this extremely low carrier concentration might be the Pb and Mg residues in the crystals; these could compensate the natural n-type doping of the material.[30] It has been recently reported that the conductivity in bulk samples is 4–5 orders of magnitude lower than in thin films, which was attributed to conductivity being dominated by surface defects.[13] A high surface conductivity is consistent with the results presented here. We observe a very high resistivity in four-point-probe measurements, yet no apparent charging in PES, LEIS, or LEED, and stable tunneling in STM. Together with the pronounced surface state observed in STS, we conclude that the surface is indeed the dominant conductivity channel.

The carrier concentration value determined in this work is probably still assessed too high to represent the intrinsic value, and it gives an upper limit for two reasons: First, we cannot exclude the possibility that even our conductivity measurements of a bulk sample may be affected by a high surface conductivity. Second, the mobility of our crystals could be higher compared to the value from the literature because of the lower impurity scattering in our crystals.

The Debye screening length λ_D of the crystal was estimated using the relation[32]

$$\lambda_D = \left(\frac{\varepsilon_0 \varepsilon_r k_b T}{n e^2}\right)^{1/2},$$

where ε_0 is the vacuum permittivity, ε_r is the relative permittivity, k_b is the Boltzmann constant, T is the temperature, n is the carrier concentration, and e is the elementary charge. For ε_r, a value of 8.9 was used.[33] Due to the low carrier concentration, the resulting Debye length in the bulk is rather large at 3.6 μm.

The bulk Fermi energy can be estimated from the bulk carrier concentration:[29]

$$E_F - E_C = \ln\left[\frac{n}{2}\left(\frac{m^* k_b T}{2\pi\hbar^2}\right)^{-\frac{3}{2}}\right] k_b T,$$

where E_F is the Fermi energy, E_C is the conduction band energy, and m^* is the effective mass of electrons in the conduction band (CB), 0.35 m_e.[33] The expected position of the Fermi level in the bulk is, therefore, ~0.4 eV below the conduction band minimum (CBM) at room temperature. Assuming a lower (higher) carrier concentration by a factor of 10 would put the bulk Fermi energy at ~0.46 eV (~0.34 eV) below the CBM.

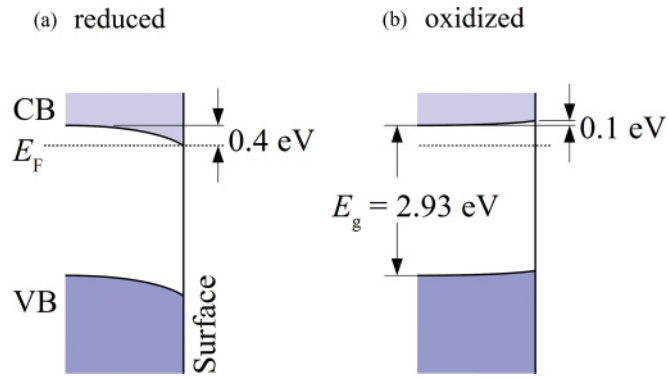

FIG. 11. (Color online) Downward band bending of the reduced surface (a) and upward band bending of the oxidized surface (b).

2. *Band bending*

There are two interesting effects regarding the electronic structure, which were observed by PES and STS, namely, a rigid shift in the core levels and gap states. Both depend on the sample preparation conditions. A more-or-less rigid shift of the VB (Fig. 8) and all core levels [Figs. 9(a) and 9(b)] indicates band bending. We can derive the band bending from the VBM determined from PES (E_F −2.9 and 2.4 eV for the reduced and oxidized surfaces, respectively), the band gap, and the position of the Fermi level with respect to the CBM in the bulk, which we have calculated as −0.4 eV (Sec. III B 1). Assuming a fundamental band gap of 2.93 ± 0.15 eV,[7] the Fermi level is located 2.5 eV above the VBM in the bulk. This means that the bands are bent downward by 0.4 eV at the reduced surface, with the CBM just reaching the Fermi level at the surface (Fig. 11). For the oxidized surface, the data indicate a very small band bending of 0.1 eV in the upward direction, which is less than the uncertainties of the underlying data (fundamental band gap and Fermi level in the bulk). Thus, the data are also consistent with a vanishing band bending on the oxidized surface.

For the reduced surface, the band bending could be explained as Fermi level pinning by gap states close to the CBM or simply the excess of positive charge (excess of indium cations) at the surface, even in the absence of gap states. Our PES data show that the gap states are mainly close to the VBM, with only a slight tail extending toward energies near the CBM, and thus it is unclear whether the gap states are responsible for the band bending.

The large Debye length of 3.6 μm calculated for the bulk of our samples implies that the band bending reaches far into the bulk. However, the carrier concentration at the surface should be higher due to the band bending (E_F closer to the CBM), which would decrease the screening length. Nevertheless, no reduction of the band bending is observable when increasing the photon energy, i.e., lowering surface sensitivity of the PES measurement, indicating that the screening length at the surface is still larger than a few monolayers.

Band bending in In_2O_3 has been reported previously. King *et al.*[4] described a downward band bending of 0.3 eV determined by x-ray photoelectron spectroscopy (XPS) for thin films grown by plasma-assisted molecular beam epitaxy (PAMBE) on YSZ. This value was revised later to

0.45 ± 0.16 eV due to better knowledge of the band gap and an alternative method of analysis.[7] Both, the surface E_F and the bulk E_F are above the CBM, which allowed them to see weak emissions by occupied CB states in XPS.

Klein[34] observed that higher oxygen pressure during deposition leads to a lower Fermi level position in the band gap, which is the same trend as for our results, but the energy differences between the VBM and E_F showed a slightly larger spread (2.5 to 3.1 eV). Since he assumed a band gap of 3.6 eV, he explained the PES results with an upward band bending in the order of 1 eV, which would lead to a surface depletion layer.

Bierwagen *et al.*[35] described a downward band bending by 0.2 eV for a thin film (plasma-assisted MBE on YSZ). After exposing the film to oxygen plasma, an upward band bending by 0.65 eV was observed.

3. *Surface states*

In general, the VB of In_2O_3 is dominated by O *2p*-derived states with a lower VB peak from In *5s*.[1,18,24,36–38] The CB is dominated by the In *5s* states. Gap states of pure In_2O_3 have been reported previously. Klein investigated the surface of reactively evaporated In_2O_3 films *in situ* by using synchrotron-excited photoemission.[34] He observed gap states depending on the oxygen pressures while preparing the films. He describes an increasing intensity of the gap states with decreasing pressure, which goes along with an increase of the optical absorption. He concluded that these gap states have their origin in different stoichiometries.

Agoston and Albe calculated the electronic structure of the reduced, stoichiometric, and the full peroxide termination.[18] The fully reduced (metallic) surface shows In *5s*-derived, half-filled metallic gap states, which should have an acceptor character and, therefore, cause an upward band bending. For the stoichiometric surface, they predict—similar to Walsh and Catlow[1]—a split-off feature from the O *2p* states close to the VBM, which is caused by undercoordinated oxygen atoms. For the surface under oxidizing conditions, peroxide surface states appear in the band gap coming from the anti-bonding p$-\pi$ orbitals of the dimers. Other distinctive features for this termination are the bonding p$-\sigma$ orbitals at the bottom of the VB and an ∼5 eV splitting of the O *2s* states of the dimers.

As shown in Fig. 8(a), the reduced surface shows low-lying gap states at ∼2.4 eV and ∼1.8 eV. Figure 8(b) shows the VB of the reduced surface at different photon energies. The gap states apparently decrease with increasing energy. This indicates that the gap states are located at the surface. At first glance, these might be identified as the In *5s* states of a fully indium-terminated surface calculated by Agoston and Albe, but this calculation shows partly filled states, which does not fit the position of the Fermi level at the CBM. The gap states should be consequently attributed to a structure with oxidic (ionic), not metallic, indium. Another interesting feature of Fig. 8(b) is the decrease of the VB peak at $\sim E_F - 8.5$ eV with increasing photon energy, again pointing toward an origin of this peak at the surface. According to the electronic density of states (EDOS) calculations, this peak should mainly arise from the In *5s* states. Therefore, it represents another argument for an indium termination.

As E_F at the surface is very close to the CBM, the state measured with STS at E_F (Fig. 7) could be either a surface state or the edge of the CB. We believe that it cannot be the CB edge alone, because in this case we would expect a higher slope below E_F. Unfortunately, this surface state could not be confirmed by PES. There are two plausible explanations for this: First, STS is most sensitive for surface states at $\overline{\Gamma}$ ($k_{||} = 0$). The PES analyzer had a rather wide acceptance angle of $\theta = 12^\circ$. The measurable parallel component with this setup can be determined by:

$$k_{||} = \sqrt{\frac{2m_e E_{\text{kin}}}{\hbar^2}} \sin\frac{\theta}{2}.$$

This leads to the result that reciprocal-space areas of $k_{||}^2\pi = 0.95\,\text{Å}^{-2}$ (photon energy: 105 eV) or $1.67\,\text{Å}^{-2}$ (photon energy 185 eV) are covered. Therefore, the analyzer collects electrons from an area larger than the first Brillouin zone (BZ): $(\frac{2\pi}{a})^2 = 0.39\,\text{Å}^{-2}$. A state at $\overline{\Gamma}(k_{||} = 0)$ might not be visible if it comprises only a small fraction of the first BZ. Assuming that the state observed by STS is located close to E_F, has a parabolic dispersion, and energy of ΔE from the bottom of the band to E_F, we can estimate the fraction of the BZ occupied by this state:

$$k_{||} = \sqrt{\frac{2m^* E_{\text{kin}} \Delta E}{\hbar^2}}.$$

With an effective mass equal to that of the In_2O_3 CB ($m^* = 0.35m_e$)[30] and assuming $\Delta E = 2k_B T$ at 300 K, the state below E_F occupies only ∼1% of the reciprocal-space area measured by the PES analyzer.

The second argument is related to the cross sections. The results from Agoston and Albe suggest that the surface state probably arises from In *5s* states.[18] According to the literature, the In *5s* photoionization cross sections should be rather small compared to the ones for O *2p* (∼6.7% at 105 eV photon energy).[21] Even at 185 eV—where the In *5s* cross section is about 25% of the O *2p* cross section—the surface state could not be observed. Indeed, angle-resolved photoemission spectroscopy (ARPES) measurements of surface states close to E_F derived from In *5s* are typically taken with a much lower photon energy of ∼10 eV.[39]

The oxidized surface does not exhibit gap states in PES, contrary to what we would have expected from the DFT calculations:[18] Neither the predicted O *2s* splitting and the orbital at the bottom of the VB (full peroxide termination) nor the gap states for the undercoordinated oxygen (partly peroxide surface) could be observed. Besides the roughness on the atomic level, this is a further indication that the oxidized surface, though probably stoichiometric, has a different structure than assumed in the calculations.

IV. CONCLUSIONS

The bulk and surface properties of In_2O_3(001) single crystals have been investigated. The flux-grown samples allowed us to determine the bulk lattice constant and crystal structure by XRD with high precision. Residues of Pb, Mg, and Pt were found in the In_2O_3 crystals. Different from thin films and polycrystalline samples investigated so far, our

samples are characterized by a low bulk carrier concentration of $\approx 10^{12}$ cm^{-3}.

Sputtering and annealing in UHV up to a maximum temperature of 500 °C (higher temperatures cause an irreversible orange discoloration attributed to oxygen loss) likely produce indium-terminated surfaces, which are characterized by low-lying gap states at ∼2.4 eV and ∼1.8 eV located at the surface. The position of the VBM at a binding energy of 2.9 eV implies a strong downward band bending by 0.4 eV. A pronounced surface state was observed in STS.

When the surfaces are exposed to activated oxygen, the electronic structure changes. The low-lying band gap states disappear, and the downward band bending is removed or even slightly reversed. A shoulder at the O *1s* core level may indicate the presence of peroxo species, albeit with a rather low surface concentration.

STM shows the presence of wide terraces that are separated by 5-Å-high step edges for both the reduced and the oxidized surfaces. The terraces of the reduced surface are covered with small 2.5-Å-high islands showing atom-sized features in a square pattern aligned with the [110] direction. Possibly, the lower terrace consists of an M-layer with small islands of D-layer indium atoms. This fact may be related to a charge compensation mechanism as observed on ZnO.[26] Similar surface energies for the M- and D-layers as calculated in a recent DFT study[18] are a prerequisite for such a structure, but the models considered so far are not consistent with our data. The oxidized surface shows even larger roughness on the atomic scale than the reduced surface.

Measurements with surface spectroscopies and STM were not hampered by charging effects despite the low bulk conductivity of the crystals. In combination with a pronounced surface state located at E_F and band bending with the Fermi level pinned close to the CBM, this strongly points to a surface-dominated conductivity in pure In_2O_3 (reduced surface), in agreement with recent literature.[13]

ACKNOWLEDGMENTS

This work was supported in part by the Austrian Science Fund (FWF; project F45) and the US Department of Energy. Research at the Oak Ridge National Laboratory for one author (L.A.B.) is sponsored by the US Department of Energy, Basic Energy Sciences, Materials Sciences and Engineering Division. Single crystal data were kindly provided by Berthold Stöger and the XRD center Vienna. This work was also supported by the Swedish Research Council, the Crafoord Foundation, the Knut and Alice Wallenberg Foundation, the Foundation for Strategic Research (SSF) and the Anna and Edwin Berger Foundation. Useful discussions with Péter Ágoston und Karsten Albe are gratefully acknowledged.

*diebold@iap.tuwien.ac.at

[1] A. Walsh and C. R. A. Catlow, J. Mater. Chem. **20**, 10438 (2010).
[2] T. Bielz, H. Lorenz, W. Jochum, R. Kaindl, F. Klauser, B. Kloetzer, and S. Penner, J. Phys. Chem. C **114**, 9022 (2010).
[3] V. Golovanov, M. A. Mäki-Jaskari, T. T. Rantala, G. Korotcenkov, V. Brinzari, A. Cornet, and J. Morante, Sens. Actuat. B (Chemical) **106**, 563 (2005).
[4] P. D. C. King, T. D. Veal, D. J. Payne, A. Bourlange, R. G. Egdell, and C. F. McConville, Phys. Rev. Lett. **101**, 116808 (2008).
[5] C. Janowitz, V. Scherer, M. Mohamed, A. Krapf, H. Dwelk, R. Manzke, Z. Galazka, R. Uecker, K. Irmscher, R. Fornari, M. Michling, D. Schmeißer, J. R. Weber, J. B. Varley, and C. G. van de Walle, New J. Phys. **13**, 085014 (2011).
[6] R. L. Weiher and R. P. Ley, J. Appl. Phys. **37**, 299 (1966).
[7] P. D. C. King, T. D. Veal, F. Fuchs, C. Y. Wang, D. J. Payne, A. Bourlange, H. Zhang, G. R. Bell, V. Cimalla, O. Ambacher, R. G. Edgell, F. Bechstedt, and C. F. McConville, Phys. Rev. B **79**, 205211 (2009).
[8] E. H. Morales, Y. He, M. Vinnichenko, B. Delley, and U. Diebold, New J. Phys. **10**, 125030 (2008).
[9] E. H. Morales and U. Diebold, Appl. Phys. Lett. **95**, 253105 (2009).
[10] A. Bourlange, D. J. Payne, R. G. Palgrave, J. S. Foord, R. G. Egdell, R. M. J. Jacobs, A. Schertel, J. L. Hutchison, and P. J. Dobson, Thin Solid Films **517**, 4286 (2009).
[11] J. H. W. De Wit, J. Solid State Chem. **13**, 192 (1975).
[12] P. Ágoston, P. Erhart, A. Klein, and K. Albe, J. Phys. Condens. Matt. **21**, 455801 (2009).
[13] S. Lany, A. Zakutayev, T. O. Mason, J. F. Wager, K. R. Poeppelmeier, J. D. Perkins, J. J. Berry, D. S. Ginley, and A. Zunger, Phys. Rev. Lett. **108**, 016802 (2012).
[14] P. Ágoston and K. Albe, Phys. Rev. B **81**, 195205 (2010).
[15] M. Marezio, Acta Crystallogr. **20**, 723 (1966).
[16] P. W. Tasker, J. Phys. C **12**, 4977 (1979).
[17] J. Goniakowski, F. Finocchi, and C. Noguera, Rep. Prog. Phys. **71**, 016501 (2008).
[18] P. Agoston and K. Albe, Phys. Rev. B **84**, 045311 (2011).
[19] S. R. Hall, H. D. Flack, and J. M. Stewart, *Xtal 3.2 Reference Manual and User's Guide* (Universities of Western Australia, Geneva and Maryland, 1992).
[20] L. E. Halliburton, N. C. Giles, N. Y. Garces, M. Luo, C. Xu, L. Bai, and L. A. Boatner, Appl. Phys. Lett. **87**, 172108 (2005).
[21] R. Nyholm, J. N. Andersen, U. Johansson, B. N. Jensen, and I. Lindau, Nucl. Instrum. Meth. Phys. Res. A **467**, 520 (2001).
[22] J. J. Yeh and I. Lindau, At. Data Nucl. Data Tables **32**, 1 (1985).
[23] S. A. Chambers, T. Droubay, T. C. Kaspar, and M. Gutowski, J. Vac. Sci. Technol. B **22**, 2205 (2004).
[24] C. Zhou, J. Li, S. Chen, J. Wu, K. R. Heier, and H. Cheng, J. Phys. Chem. C **112**, 14015 (2008).
[25] Y. Gassenbauer, R. Schafranek, A. Klein, S. Zafeiratos, M. Hävecker, A. Knop-Gericke, and R. Schlögl, Phys. Rev. B **73**, 245312 (2006).
[26] O. Dulub, U. Diebold, and G. Kresse, Phys. Rev. Lett. **90**, 016102 (2003).
[27] O. Bierwagen, M. E. White, M. Y. Tsai, and J. S. Speck, Appl. Phys. Lett. **95**, 262105 (2009).
[28] K. H. L. Zhang, A. Walsh, C. R. A. Catlow, V. K. Lazarov, and R. G. Egdell, Nano Lett. **10**, 3740 (2010).

[29]C. Kittel, *Einführung in die Festkörperphysik*, 8th ed. (Oldenbourg, München, 1989).
[30]O. Bierwagen and J. S. Speck, Appl. Phys. Lett. **97**, 072103 (2010).
[31]J. De Wit, J. Solid State Chem. **20**, 143 (1977).
[32]P. Y. Yu and M. Cardona, *Fundamentals of Semiconductors*, 4th ed. (Springer, Heidelberg, 2010).
[33]I. Hamberg and C. G. Granqvist, J. Appl. Phys. **60**, R123 (1986).
[34]A. Klein, Appl. Phys. Lett. **77**, 2009 (2000).
[35]O. Bierwagen, J. S. Speck, T. Nagata, T. Chikyow, Y. Yamashita, H. Yoshikawa, and K. Kobayashi, Appl. Phys. Lett. **98**, 172101 (2011).
[36]F. Fuchs and F. Bechstedt, Phys. Rev. B **77**, 155107 (2008).
[37]L. A. Errico, M. Rentería, G. Fabricius, and G. N. Darriba, Hyperfine Interact. **158**, 63 (2004).
[38]P. Erhart, A. Klein, R. Egdell, and K. Albe, Phys. Rev. B **75**, 153205 (2007).
[39]K. H. L. Zhang, Ph.D. thesis, University of Oxford, Oxford, UK, 2011.